Activation Mechanism of Nickel(0) *N*-Heterocyclic Carbene Catalysts Stabilized by Fumarate Ligands

Michael T. Robo, Amie R. Frank, Ellen Butler, Alex J. Nett, Santiago Cañellas, Paul M. Zimmerman,* and John Montgomery*

Department of Chemistry, University of Michigan, Ann Arbor, MI 48109-1055, USA

Abstract: Nickel(0) catalysts of *N*-heterocyclic carbenes (NHCs) that are stabilized by electronic deficient alkenes possess desirable properties of air tolerance and ease of handling while also retaining high catalytic activities. Since catalyst stability often comes at the expense of catalytic activity, we have undertaken a detailed study of the activation mechanism of an IMes-nickel(0) catalyst stabilized by di-(*o*-tolyl) fumarate that converts the stable pre-catalyst form into a catalytically active species. Computational evaluation provided evidence against a simple ligand exchange as the activation mechanism for this catalyst, and a stoichiometric activation process that covalently modifies the stabilizing ligand was identified. A detailed computational picture for the activation process was developed, with predictive insights that elucidate an unexpected catalyst activation pathway that operates when ligand exchange is thermodynamically unfavorable.

INTRODUCTION

A vast array of synthetic methods involving nickel catalysis has been developed in recent years.[1] Methods that involve exogeneous reductants often are best accomplished with air-stable Ni(II) catalysts,[1d,e] which are desirable compared with more air-sensitive Ni(0) counterparts. While processes involving phosphine and pyridine ligand frameworks often perform well with Ni(II) precursors,[2] reactions that involve *N*-heterocyclic carbene ligands are more commonly performed with $Ni(COD)_2$ as the precatalyst. This choice is due to inefficiencies in the catalyst reduction and

formation of catalytically active Ni(0) species. At the same time, *in situ* formation of Ni(0)-NHC complexes has disadvantages of instability of Ni(0) precatalysts and NHC ligands,[3] inhibitory effects of cyclooctadiene in some classes of catalytic processes, especially C-H activation processes involving LLHT activation mechanisms,[4] and the precise control of metal-ligand stoichiometry, especially on the small scales required for high throughput experimentation.[5]

Ni(0) catalysts that are stabilized by simple alkenes have proven effective across many reaction classes, with more electron-deficient alkenes typically providing more stable but less active catalysts compared with the most commonly employed precursors such as $Ni(COD)_2$. Catalyst **1**, initially reported by Cavell,[6] includes IMes as the NHC ligand and dimethyl fumarate as the stabilizing π-acid and serves as a prototypical example of the increased stability and diminished reactivity imparted by the electron-deficient alkene additives. Recent work from our lab built upon this template and examined acrylate, fumarate, and methacrylate π-acids to refine the stability-reactivity balance.[7] While catalyst **1** possesses exceptional stability in air and performs effectively in the oxidation of secondary alcohols,[8] we found that processes including aldehyde-alkyne reductive couplings and aminations of aryl chlorides were not effective due to deactivation of the catalyst by the fumarate. Systematic variation of the NHC and stabilizing π-acid led to the identification of a number of catalysts that participate effectively with these reaction classes and rapidly initiate without a discernable induction period. Our initial observations found that the optimal π-acid depends on the NHC ligand, and the stability-reactivity continuum can be optimized according to the precise catalytic properties and stability desired. Complexes **2**-**4** were found to display excellent catalytic properties in aldehyde-alkyne reductive couplings (catalysts **2** and **3**) and aryl chloride aminations (catalyst **4**) and are now sold by commercial vendors (Figure 1).

Other classes of promising air-stable Ni(0) catalysts have subsequently been disclosed by Cornella and Engle, with Ni(0) centers stabilized by either stilbene or quinone π-acids.[9] These catalysts possess the advantage of enabling modular *in situ* coordination to different ligands, whereas the NHC/π-acid combinations have the advantage of being a single-component system with pre-defined structure and metal-ligand stoichiometry, as illustrated with electronic-deficient akenes[3,7] and other olefin classes.[4,10] We envision that the latter characteristics will offer unique advantages with NHC catalysts in high-throughput arrayed methods where inefficient mixing and imprecise control of metal-ligand stoichiometry are avoided with a single-component, well-defined catalyst source.

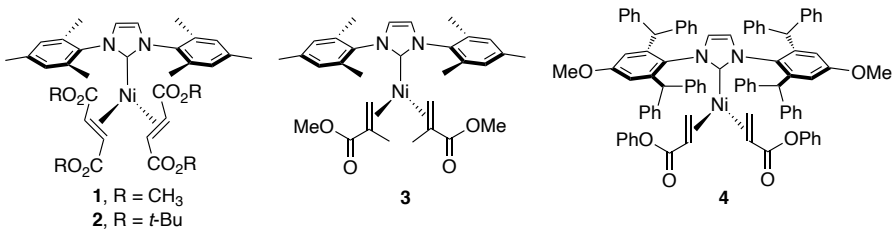

Figure 1. First generation stable Ni(0) NHC complexes. CAS numbers: **2**: 2230140-59-5, **3**: 2230140-51-7, **4**: 2230140-52-8.

Prior studies from numerous laboratories have illustrated that judicious choice of alkene ligands can play a key role in tuning the stability and reactivity of numerous families of Ni(0) catalysts, a current gap in the field is the understanding of how Ni(0) complexes stabilized by simple ligands undergo activation to more active forms of the catalyst. A question that remains unanswered for most Ni(0) precatalysts is whether simple ligand dissociation affords active catalyst forms, or if more complex activation steps involving chemical modification of the alkene are required. We have now studied this question in detail with fumarate catalysts that build on the design features of an NHC ligand paired with a π-acid selected to balance stability and reactivity. In this study, the fate of the stabilizing alkene ligand and mechanism of catalyst activation are

elucidated through experimental and computational studies that evaluated different mechanisms for catalyst activation, including displacement as well as covalent sequestration of the stabilizing π-acid.

RESULTS AND DISCUSSION

Our initial report described the activity of catalysts **2-4** among other nickel(0) NHC complexes stabilized by electron-deficient alkenes and suggested that the stability-reactivity continuum could be tuned to achieve desired catalyst properties.[7] In particular, fumarates with especially high binding affinity to nickel are expected to stabilize the resulting complex, but likely inhibit productive catalysis. Conversely, weakly bound fumarates would lead to unstable precatalysts, which would degrade prior to use in catalysis. When framed in this way, the thermodynamic affinity of fumarate to nickel takes a central role and leads to a key initial hypothesis: ligand exchange governs the stability-reactivity continuum for these precatalysts. In order to test this hypothesis and use this information to improve this family of catalysts, we set out to better understand the chemical principles that govern the relationship of stability and reactivity. The design strategy, based on this thermodynamic rationale, was to tune the fumarate binding affinity to offset the innate electronic stabilization of the electron-deficient alkene by steric interactions with the NHC. Specifically, we wanted to locate a region in chemical space where the fumarate ligand would be bound loosely enough to allow for reactivity, but also be bound strongly enough to maintain air-stability.

Evaluating the Thermodynamic Dissociation Hypothesis

To test whether the thermodynamics of ligand binding were controlling the activation of the Ni(0) NHC complexes, seven different fumarate complexes of IMes (**1-2**, **5-10**, Figure 2) with varying electronics and sterics were considered. In the model reaction of 4-fluorobenzaldehyde

(**12**) and phenyl propyne (**13**) using triethylsilane as the reductant, a potential first step for activation of the Ni complex is displacement of the two fumarate ligands with aldehyde and alkyne. We computed the free energy of fumarate ligand exchange with the aldehyde and alkyne reaction components using eight representative fumarate complexes and compared their binding affinities to Cavell's original complex (**1**) (Table 1). Complex **1** was chosen as a reference point for this series, as it is known to be air-stable and was observed to be unreactive in the reductive couplings of aldehydes and alkynes and in aryl chloride aminations.[7] We anticipated that if the mechanism of catalyst activation simply involves exchange of the fumarate **16** for the aldehyde and alkyne components (**12** and **13**), then the catalysts with lowest free energy of exchange will most easily reach the active catalyst state, i.e., Ni(0) free of the stabilizing fumarate ligand. As seen in Table 1, the complexes examined were found to have similar or higher fumarate binding affinities, relative to **1**, with the exception of di-(*t*-butyl) fumarate complex **2**. While the ordering of binding energies for catalysts 5 and 6 is contrary expectations based on steric trends, the differences in energies are within the expected range of error, and the increased surface area of catalyst **6** vs **5**, allowing for more Van der Waals interactions during complexation, may be the origin of the small computed difference.

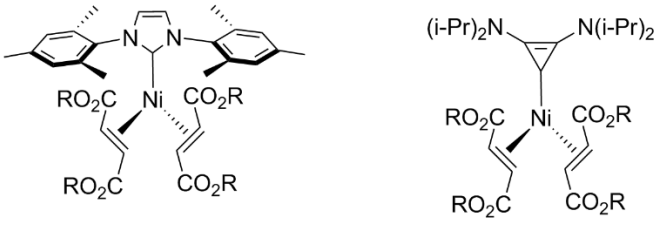

1, R = CH_3
2, R = *t*-Bu
5, R = Et
6, R = *i*-Pr
7, R = *o*-tol
8, R = *o*-$(C_6H_4)OCH_3$
9, R = *p*-$(C_6H_4)OCH_3$
10, R = *p*-$(C_6H_4)CO_2CH_3$

11, R = *o*-tol

Figure 2. Catalyst structures used in this study

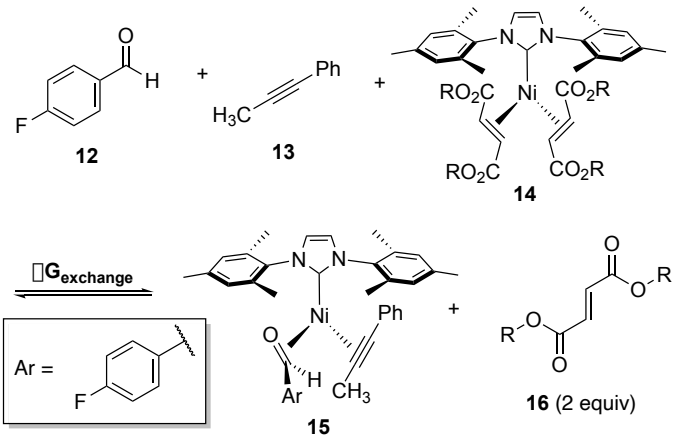

Catalyst	R group	ΔG exchange relative to 1 (kcal/mol)
1	Me	0.0 (reference)
2	*t*-Bu	-6.0
5	Et	-1.7
6	*i*-Pr	-0.5
7	*o*-tol	14.4
8	*o*-(C_6H_4)OCH_3	8.3
9	*p*-(C_6H_4)OCH_3	10.2
10	*p*-(C_6H_4)CO_2CH_3	12.3

Table 1. Computed free energy of ligand exchange. Free energies are calculated from ωB97X-D3/cc-pVTZ/THF. Absolute binding energies are available in the SI.

The hypothesis of catalyst activation through purely thermodynamic control considered with the relative binding energies from Table 1 suggests that the fumarate complexes **7**-**10** would be as inactive as complex **1** in reductive coupling reactions. Regardless, the increased steric bulk of the fumarates compared to **1** and variations in electronics of the aryl groups of **7-10** provided a significant range of binding energies. Therefore, this set could be used to better understand the relationship between fumarate binding and reactivity, and we experimentally tested a representative set of the compounds evaluated by computation. The model coupling reaction (Figure 3, top)

was performed for representative precatalysts and monitored by ^{19}F NMR. Across the catalyst series **1-2** and **5-10**, all of the tested fumarate complexes except for catalyst **10** were found to be more active than the parent dimethyl fumarate complex **1** (see SI). Figure 3 shows that the rates and conversions were highest for those catalysts that possessed the bulkiest fumarate substituents (**2**, **6**, **7**).

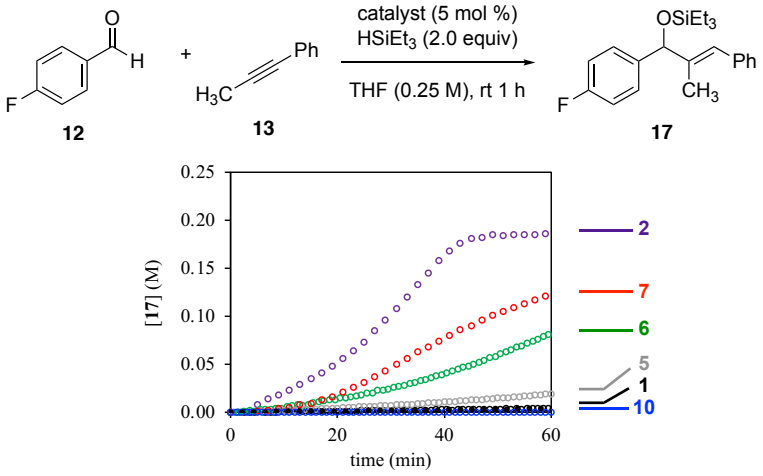

Figure 3. Reaction progression plots for select catalysts using ^{19}F NMR. Catalysts **2**, **7**, and **6** showed the most activity (see Figure 2 for structures).

The reactivity ordering in Figure 3 showed no clear relationship to the binding affinities detailed in Table 1. This is also true when looking at only exchanging a single fumarate for an alkyne or aldehyde (page S26 of SI). While the most reactive catalyst **2**, which possesses a di-(*t*-butyl) fumarate ligand, also has the most favorable exchange energy for the **14** to **15** conversion, other complexes such *o*-tol precatalyst **7** exhibited excellent catalytic reactivity at room temperature, despite having a fumarate binding affinity that is too endergonic to undergo the **14** to **15** exchange under the reaction conditions (>14 kcal/mol above that of **1**). This means that if ligand

exchange were a necessary step for catalyst activation, **7** should be completely inactive. Furthermore, the positive curvature of catalysts **2**,**6**, and **7** suggested that some form of catalyst activation sequence occurs.

In addition to the precatalysts of Table 1, smaller carbenes such as the *i*-Pr-BAC cyclopropenylidene ligands were of interest to our group, as they have proven unique in related applications.[11] Catalyst **11**, however, was air stable but unreactive in aldehyde-alkyne reductive couplings. Unlike catalyst **7**, catalyst **11** was found to have a weak fumarate binding energy that was 4.2 kcal/mol uphill of catalyst **1**. The inactivity of **11**, despite having the same fumarate as active catalyst **7**, indicated that catalyst activity is not solely dependent on fumarate identity, but may also be affected by the interplay between the NHC ligand and the fumarate ligand.

These results indicate that ligand exchange is likely not the mechanism of catalyst activation for the studied series of catalysts, given the unfavorable thermodynamics of ligand exchange. Among the catalysts predicted to have unfavorable ligand exchange, catalyst **7** is particularly promising based on its stability, fast initiation, and high yielding reactions in aldehyde-alkyne reductive couplings. Based on this information, we propose an alternative hypothesis: a chemical activation event is responsible for converting precatalyst **7** into an active catalyst, where the fumarate ligand is stoichiometrically consumed.

Mechanism for Catalyst Activation

We set out to test the hypothesis of ligand consumption by identifying the fate of the fumarate in the activation process. Specifically, we examined reactions with an elevated catalyst loading to allow the fate of the fumarate ligand to be tracked. Precatalyst **7** is readily prepared from $Ni(COD)_2$, IMes, and di-(*o*-tolyl) fumarate, it possesses excellent stability and reactivity, and its structure (Figure 4) is analogous to previously reported catalyst **2**. In using 50 mol % loading

of catalyst **7** in the three-component coupling of 4-fluorobenzaldehyde, 1-phenyl propyne, and triethylsilane, product **18** was isolated. **18** might result from a four-component reductive cycloaddition including the di-(*o*-tolyl) fumarate from the nickel catalyst, and byproduct **19** was observed by GCMS analysis (Scheme 1). The process resembles Et_3B-mediated reductive cycloaddition involving enoates, alkynes, and aldehydes,[12] but has not been observed or proposed as a mechanism for catalyst activation. Given the complexity and uncertain mechanism of the formation of byproduct **18**, we turned to computational reaction pathway evaluation tools to provide a clear explanation for these phenomena.[13]

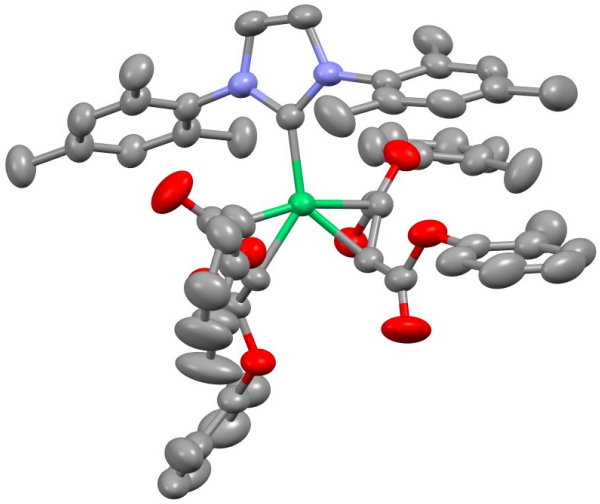

Figure 4. ORTEP diagram of complex **7** with thermal ellipsoids at 50 % probability. Hydrogen atoms are omitted for clarity.

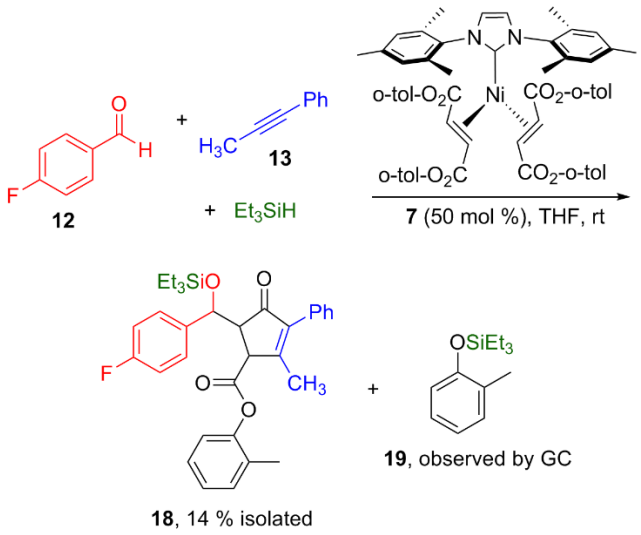

Scheme 1. Generation of products **18** and **19** in an activation pathway for catalyst **7.**

Based on analogy to our prior studies, we envisioned that **18** might derive from metallacycle **20** via oxidative cyclization of a bound fumarate ligand with an alkyne (Scheme 2). The formation of metallacycle **20** could proceed through an "aldol first" pathway[12b] involving direct addition of aldehyde to the nickel enolate of **20** to generate nickel aldolate **21**. Alternatively, a "ketene first" pathway[12c] involving aryloxy elimination from the nickel ester enolate moiety of **20** could generate ketene intermediate **22**. In either case, a cascade four-component coupling pathway combining a fumarate ligand, aldehyde, alkyne, and silane would afford products **18** and **19** while sequestering the fumarate. Once sequestered, the more active form of the catalyst would be available *in situ*. As this cascade process was predicted by computation to be essential for catalyst activation based on the energetic cost of ligand exchange, we set out to better understand the nature of the catalyst activation pathway.

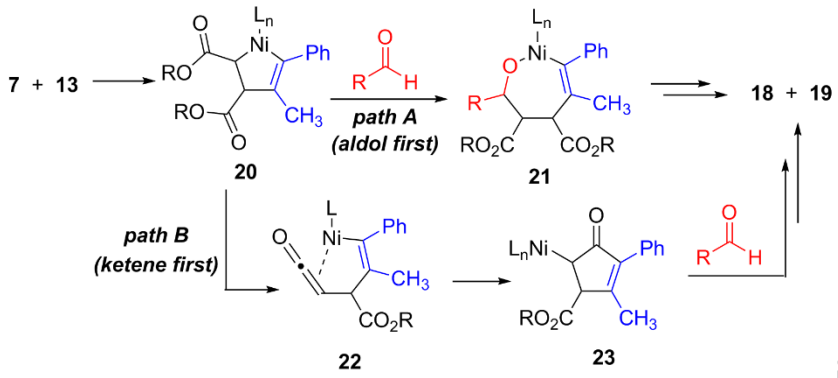

Scheme 2. Possible mechanisms for catalyst activation, leading to observed byproducts **18** and **19** (see Scheme 1).

The mechanistic details of the "aldol-first" (path A) and "ketene-first"(path B) pathways involving catalysts **7** and **11** were revealed using quantum chemical simulations (see computational details). In Figure 5, the free energy surfaces of these mechanisms for IMes catalyst **7** (pathways shown in blue and turquoise, labeled as IMes) and BAC catalyst **11** (pathways shown in red and pink, labelled as BAC) are shown. In path A (dark colors) 5-membered metallacycle **I** rotates to isomer **II**, and then isomerizes to η^3 bound **III-A** (**TS-II-A**). Complex **III-A** then isomerizes again (**TS-III-A**) to 7-membered metallacycle **IV-A**. A direct path from **I** to **IV-A** was considered, but was found to be slower for both catalysts **7** and **11** (see page S28 of SI). Alternatively, in path B (light colors), isomer **II** extrudes a unit of aryloxide (**TS-II-B**), to create ketene complex **III-B**. The ketene species can then cyclize (**TS-III-B**) to carbocyclic species **IV-B**.

To determine whether a given catalyst goes through activation path A or B, the highest energy transition states of both pathways need to be compared. In the case of catalyst **7**, with an IMes ligand, the transition state for ketene elimination (**IMes-TS-II-B**, 22.0 kcal/mol) in path B is significantly higher in energy than the highest energy transition state in path A (**IMes-TS-II-A**, 15.1 kcal/mol), which suggests that catalyst **7** undergoes activation via path A. Intriguingly, BAC-

ligated catalyst **11** has a barrier for ketene elimination (**BAC-TS-II-B**, 13.4 kcal/mol) that is significantly lower than the corresponding barrier for IMes-TS-II-B for catalyst **7**. Additionally, the barrier for isomerization from η^3 bound **BAC-III-A** (**BAC-TS-III-A**, 19.5 kcal/mol) is moderately higher than the corresponding barrier for **7** (**IMes-TS-III-A**, 13.9 kcal/mol). Taken together, the larger barrier height of **BAC-TS-III-A** (19.5 kcal/mol) compared to **BAC-TS-II-B** (13.4 kcal/mol**)** indicates that catalyst **11** prefers to undergo catalyst activation through path B. The origin of these outcomes is that the lowest energy "ketene-first" pathway proceeds through an η^1 *C*-enolate intermediate, whereas the "aldol-first" pathway requires rearrangement to an η^1 *O*-enolate intermediate. Therefore, prior to the aldol addition step itself, the energetics of the ketene formation vs *C*- to *O*- tautomerization play a key role in determining the mechanism of catalyst activation.

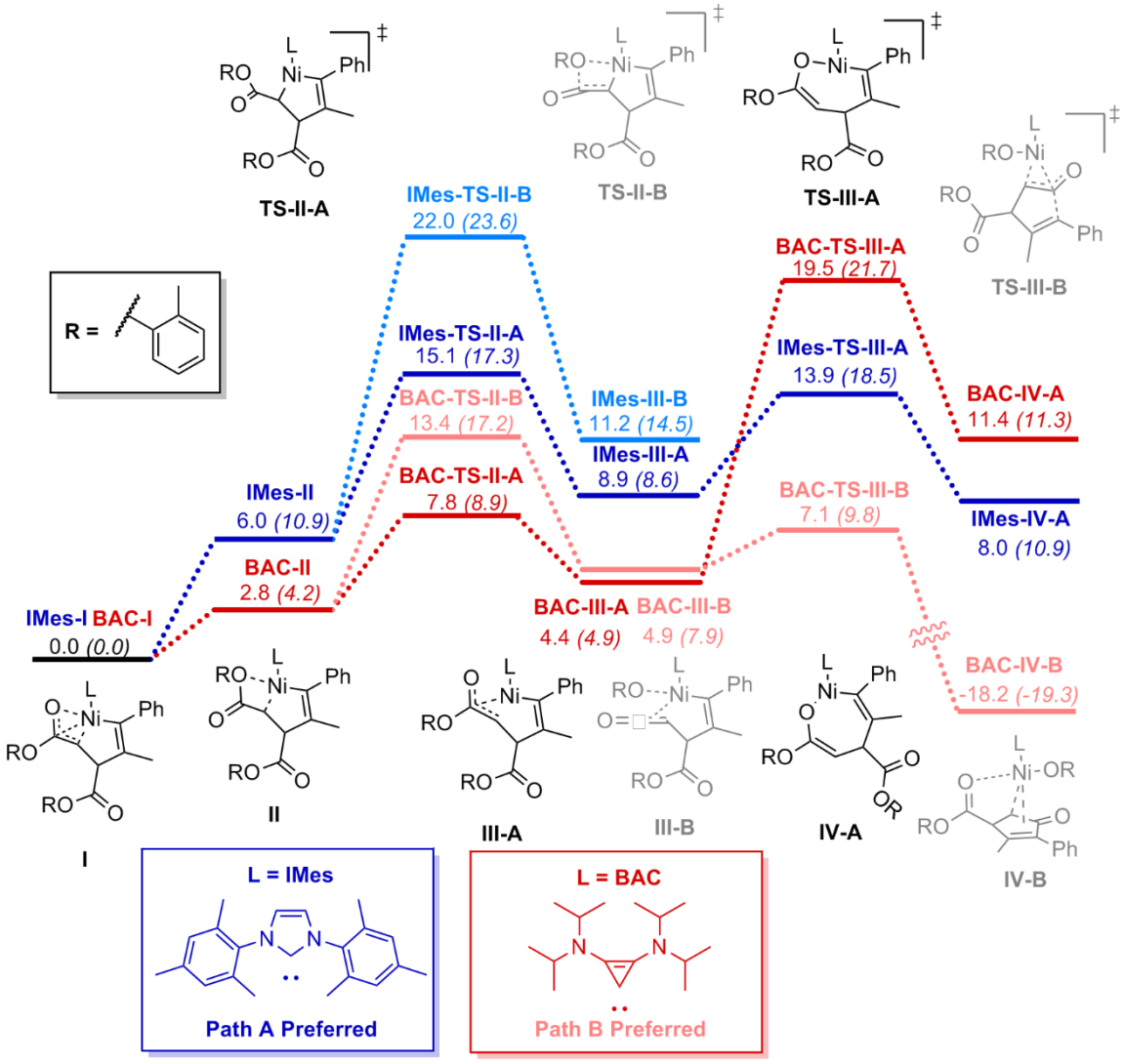

Figure 5. Free energy profile for initiation of nickel BAC and IMes complexes with di-(*o*-tolyl) fumarate. The catalyst activation sequence of BAC catalyst **11** is shown in red and in pink. The catalyst activation sequence of IMes catalyst **7** is shown in blue and turquoise. Free energies and enthalpies from ωB97X-D3/cc-pVTZ/THF are listed in kcal/mol, and enthalpy values are listed in italics. The darker colors (red, blue, and black) represent aldol-first (path A). The lighter colors (pink, turquoise, and gray) represent ketene-first (path B).

The above analysis suggests that the fumarate ligands of IMes precatalyst **7** and BAC precatalyst **11** react via different mechanisms. With this knowledge in hand, we then hypothesized

that this difference can explain why **7** is a competent catalyst, but **11** is not. To evaluate this hypothesis, we followed the progression of path A in **7** and path B in **11** along the free energy surface.

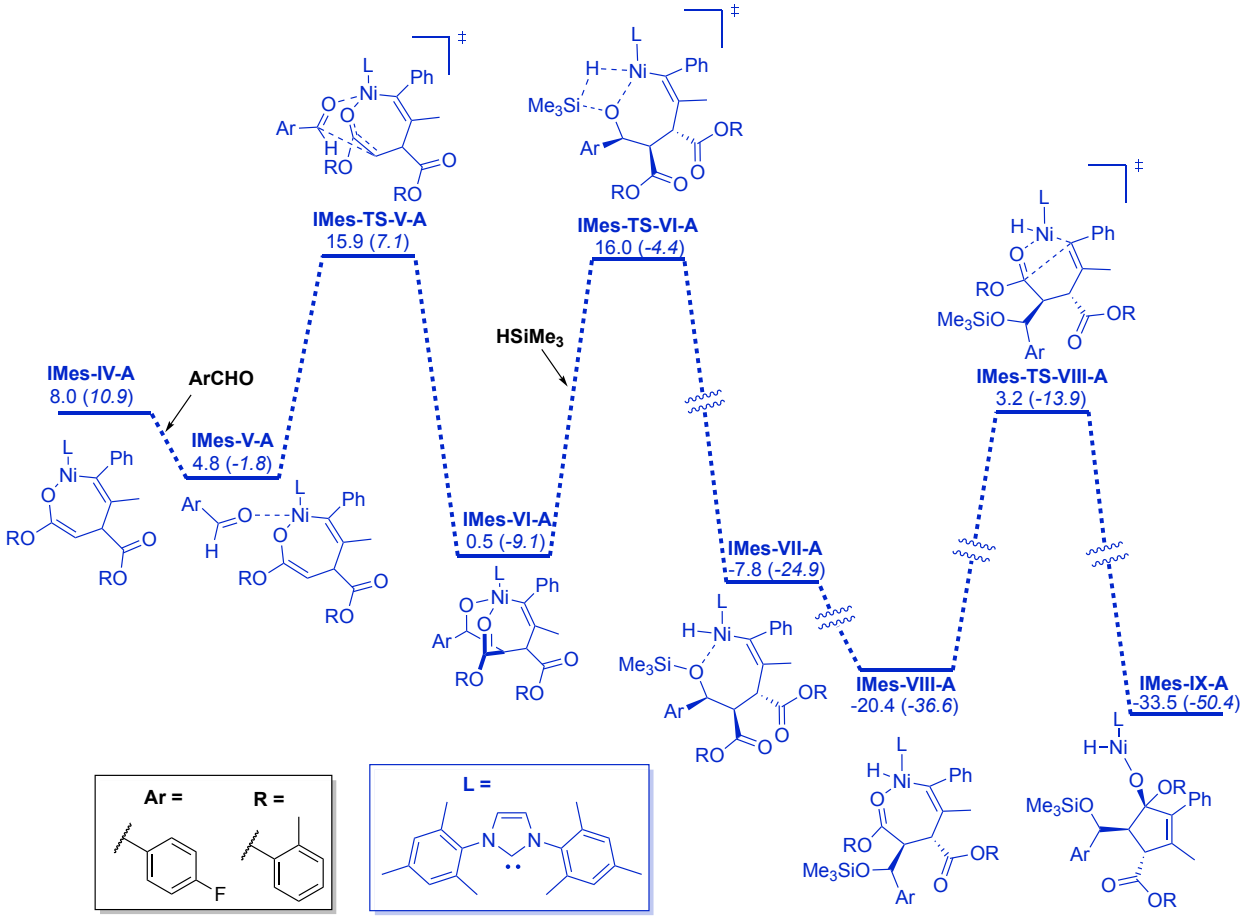

Figure 6. Free energy surface for aldol-first activation pathway of catalyst **7**. Aldol addition, hydrosilylation, and carbocyclization are shown. Free energies and enthalpies from ωB97X-D3/cc-pVTZ/THF are listed in kcal/mol, and enthalpy values are listed in italics.

In the case of catalyst **7**, path A provides a means to release a potential active catalyst. Figure 6 details the pathway for catalyst release. Seven-membered metallacycle **IMes-IV-A** can ligate to an aldehyde (**IMes-V-A**, Figure 5), and can then undergo an aldol reaction (**IMes-TS-V-A**) to yield complex **IMes-VI-A**. After aldol addition, complex **IMes-VI-A** can be subsequently hydrosilylated (**IMes-TS-VI-A**), to yield complex **IMes-VII-A**, which can rearrange to complex

IMes-VIII-A. Carbocyclization can then occur (**IMes-TS-VIII-A**, 3.2 kcal/mol), leading to nickel alkoxide species **IMes-IX-A**. This compound can easily extrude compound **18** to release a nickel alkoxy compound that can easily become the activated catalyst.

The quantum chemical results shown in Table 1 and Figures 5 and 6 can be used to explain the competency of catalyst **7** in coupling of **12** and **13.** Despite simple ligand exchange being thermodynamically unfeasible, catalyst **7** is competent in the production of allylic alcohol **17**. This implies the catalyst activation route involves consumption of the fumarate, and the catalytic activity is predicated on the formation of a byproduct such as **18** (Scheme 1). This observation motivated us to experimentally isolate compound **18** to provide a test of the fumarate consumption hypothesis. A feasible reaction pathway leading to **18** is outlined in Figures 5 and 6. In short, catalyst **7** is competent because it can undergo a reaction that removes its (strongly bound) fumarates from solution.

This observation also provides a putative reason as to why BAC catalyst **11** is incompetent in similar reductive couplings of **12** and **13**. Computational investigation of the activation pathways for **14** suggest that a ketene-first path is preferred, in contrast to the aldol-first path preferred by **11**. As a result of this change, catalyst **11** is can form highly stabilized complex **BAC-IV-B** (Figure 5). Once intermediate **BAC-IV-B** is formed, all available coordination sites are occupied, preventing aldehyde coordination and subsequent aldol addition through a closed transition state. Instead, the only pathway computationally identified for turnover of the *C*-enolate **BAC-IV-B** is a direct hydrosilylation step (Figure 7). A number of factors, however, make hydrosilylation of **BAC-IV-B** difficult. Firstly, the metal center prefers to coordinate to the nearby ester group in **BAC-IV-B**, meaning that no open coordination sites are available. Secondly, in **BAC-IV-B**, the alkoxy moiety remains *cis* to the NHC, increasing the steric bulk in the vicinity of the alkoxy

group. Finally, the large silane, $(i\text{-Pr})_3SiH$, inhibits the silylation reaction in this case. The reason for the restriction to larger silanes with the BAC ligand system relates to competing aldehyde hydrosilylation that consumes the starting aldehyde when smaller silanes are employed in combination with BAC ligands.[11a] The computed barrier for addition of $(iPr)_3SiH$ to **BAC-IV-B** illustrates that silylation via **BAC-TS-IV-B**, at 27.1 kcal/mol, is too high to be feasible at room temperature. (Figure 7). Consequently, the inertness of catalyst **14** can be ascribed to the stability of intermediate **BAC-IV-B**. In addition to the above factors that influence the activation pathway for catalyst **11**, this particular catalyst exhibits considerable stability and enters activation pathways more slowly than the corresponding IMes catalysts. Attempts to isolate fumarate byproducts in high-loading experiments with catalyst **11** akin to the experiment described in Scheme 1 afforded no identifiable fumarate-derived products.

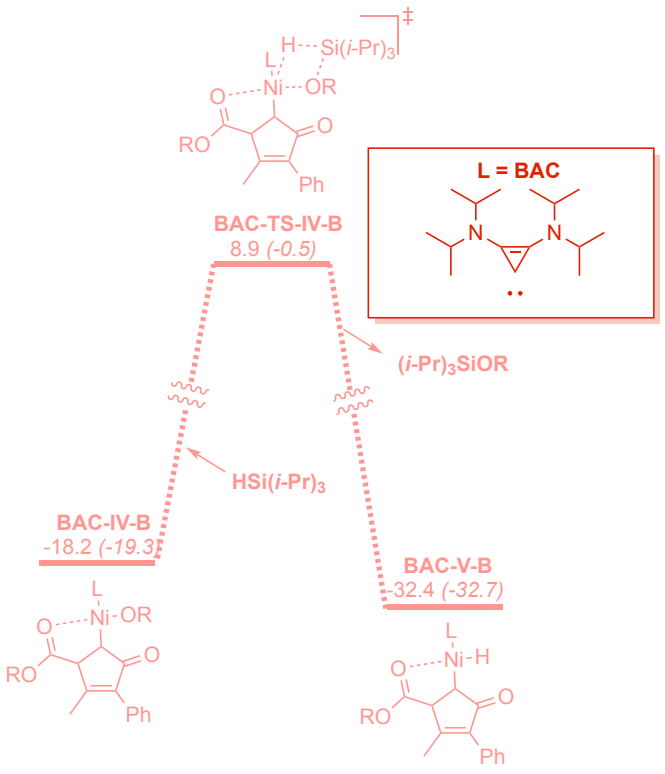

Figure 7. Free energy surface for the addition of (i-Pr)$_3$SiH a five-membered *C*-enolate using BAC as ligand.

CONCLUSIONS

In summary, we introduce a Ni(0) catalyst (**7**) complexed with IMes and two stabilizing di-(*o*-tolyl) fumarate ligands, and we demonstrate it to be a competent catalyst in the reductive coupling of aldehydes and alkynes using silanes as the terminal reductant. The catalyst is easily prepared and handled, while undergoing rapid catalyst activation under mild reaction conditions. Computational study of a panel of catalysts that range in stability and catalyst activity illustrated that simple dissociation of fumarate ligand was unlikely in some instances to serve as the catalyst activation step, as the thermodynamics of ligand exchange are uncorrelated with catalyst activity. Instead, consumption of the fumarate through a cascade cycloaddition process involving the reaction components was identified as a possible pathway for catalyst activation that allows catalysts such as **7** that cannot undergo favorable ligand exchange to nonetheless be effective catalysts. Computational studies elucidated an operative mechanism for the catalyst activation step and provided a predictive model for explaining the divergent reactivity of catalysts that possess similar structures but that undergo different activation mechanisms. The ketene elimination step in particular (**TS-II-B**) appears to have an outsized influence on path selectivity in activation. With unhindered NHC ligands such as BAC (catalyst **11**), the ketene-first pathway is predicted to lead to stable species that, in the absence of a sterically accessible silane, acts as a thermodynamic trap. Catalysts such as **7** avoid ketene formation and favor aldol-first pathways, so the steric profile of the silane is less critical for the formation of catalysts. This work continues to advance the development of highly active and well-defined Ni(0) catalysts that provide improvements in stability

and ease of handling over the corresponding structures obtained through *in situ* catalyst preparations.[14]

ASSOCIATED CONTENT

Supporting Information. Experimental and computational details. This material is available free of charge via the Internet at http://pubs.acs.org. Experimental and computational details, X-Ray crystallographic data, copies of spectra.

AUTHOR INFORMATION

Corresponding authors

****John Montgomery, jmontg@umich.edu***

****Paul M. Zimmerman, paulzim@umich.edu***

Notes

The authors declare no competing financial interests.

ACKNOWLEDGEMENTS

JM dedicates this manuscript to Prof. Maurice Brookhart in appreciation for teaching his passion for organometallic chemistry during JM's undergraduate research experience at UNC. PMZ thanks the NIH (R35-GM-128830) and JM thanks the National Science Foundation (CHE-1954939) for support for this research. JM is grateful for the mentorship from Maurice Brookhart during his undergraduate research experience at UNC Chapel Hill. The authors thank Dr. Jeff W. Kampf for crystallographic analysis of structure **7** and Mr. Austin Ventura and Mr. Mo Chen for technical assistance.

REFERENCES

1. (a) Montgomery, J., Organonickel Chemistry. In *Organometallics in Synthesis, Fourth Manual*, Lipshutz, B. H., Ed. John Wiley & Sons, Inc.: Hoboken, N. J. , 2013; pp 319-428; (b) Montgomery, J., Nickel-Catalyzed Reductive Cyclizations and Couplings. *Angew. Chem. Int. Ed.* **2004,** *43*, 3890-3908; (c) Tasker, S. Z.; Standley, E. A.; Jamison, T. F., Recent Advances in

Homogeneous Nickel Catalysis. *Nature* **2014,** *509*, 299-309; (d) Everson, D. A.; Weix, D. J., Cross-Electrophile Coupling: Principles of Reactivity and Selectivity. *J. Org. Chem.* **2014,** *79*, 4793-4798; (e) Poremba, K. E.; Dibrell, S. E.; Reisman, S. E., Nickel-Catalyzed Enantioselective Reductive Cross-Coupling Reactions. *ACS Catal.* **2020,** *10*, 8237-8246; (f) Rosen, B. M.; Quasdorf, K. W.; Wilson, D. A.; Zhang, N.; Resmerita, A. M.; Garg, N. K.; Percec, V., Nickel-Catalyzed Cross-Couplings Involving Carbon-Oxygen Bonds. *Chem. Rev.* **2011,** *111*, 1346-1416; (g) Zuo, Z.; Ahneman, D. T.; Chu, L.; Terrett, J. A.; Doyle, A. G.; MacMillan, D. W. C., Merging Photoredox with Nickel Catalysis: Coupling of Alpha-Carboxyl sp(3)-Carbons with Aryl Halides. *Science* **2014,** *345*, 437-440.

2. (a) Shields, J. D.; Gray, E. E.; Doyle, A. G., A Modular, Air-Stable Nickel Precatalyst. *Org. Lett.* **2015,** *17*, 2166-2169; (b) Standley, E. A.; Jamison, T. F., Simplifying Nickel(0) Catalysis: An Air-Stable Nickel Precatalyst for the Internally Selective Benzylation of Terminal Alkenes. *J. Am. Chem. Soc.* **2013,** *135*, 1585-1592; (c) Lavoie, C. M.; MacQueen, P. M.; Rotta-Loria, N. L.; Sawatzky, R. S.; Borzenko, A.; Chisholm, A. J.; Hargreaves, B. K. V.; McDonald, R.; Ferguson, M. J.; Stradiotto, M., Challenging Nickel-Catalysed Amine Arylations Enabled by Tailored Ancillary Ligand Design. *Nat. Commun.* **2016,** *7*, 11073; (d) Park, N. H.; Teverovskiy, G.; Buchwald, S. L., Development of an Air-Stable Nickel Precatalyst for the Amination of Aryl Chlorides, Sulfamates, Mesylates, and Triflates. *Org. Lett.* **2014,** *16*, 220-223; (e) Magano, J.; Monfette, S., Development of an Air-Stable, Broadly Applicable Nickel Source for Nickel-Catalyzed Cross-Coupling. *ACS Catal.* **2015,** *5*, 3120-3123; (f) MacQueen, P. M.; Tassone, J. P.; Diaz, C.; Stradiotto, M., Exploiting Ancillary Ligation to Enable Nickel-Catalyzed C-O Cross-Couplings of Aryl Electrophiles with Aliphatic Alcohols. *J. Am. Chem. Soc.* **2018,** *140*, 5023-5027.

3. Todd, D. P.; Thompson, B. B.; Nett, A. J.; Montgomery, J., Deoxygenative C-C Bond-Forming Processes Via a Net Four-Electron Reductive Coupling. *J. Am. Chem. Soc.* **2015,** *137*, 12788-12791.

4. Nett, A. J.; Zhao, W. X.; Zimmerman, P. M.; Montgomery, J., Highly Active Nickel Catalysts for C-H Functionalization Identified through Analysis of Off-Cycle Intermediates. *J. Am. Chem. Soc.* **2015,** *137*, 7636-7639.

5. Mennen, S. M.; Alhambra, C.; Allen, C. L.; Barberis, M.; Berritt, S.; Brandt, T. A.; Campbell, A. D.; Castañón, J.; Cherney, A. H.; Christensen, M.; Damon, D. B.; Eugenio de Diego, J.; García-Cerrada, S.; García-Losada, P.; Haro, R.; Janey, J.; Leitch, D. C.; Li, L.; Liu, F.; Lobben, P. C.; MacMillan, D. W. C.; Magano, J.; McInturff, E.; Monfette, S.; Post, R. J.; Schultz, D.; Sitter, B. J.; Stevens, J. M.; Strambeanu, I. I.; Twilton, J.; Wang, K.; Zajac, M. A., The Evolution of High-Throughput Experimentation in Pharmaceutical Development and Perspectives on the Future. *Org. Process Res. Dev.* **2019,** *23*, 1213-1242.

6. Clement, N. D.; Cavell, K. J.; Ooi, L.-l., Zerovalent N-Heterocyclic Carbene Complexes of Palladium and Nickel Dimethyl Fumarate: Synthesis, Structure, and Dynamic Behavior. *Organometallics* **2006,** *25*, 4155-4165.

7. Nett, A. J.; Canellas, S.; Higuchi, Y.; Robo, M. T.; Kochkodan, J. M.; Haynes, M. T.; Kampf, J. W.; Montgomery, J., Stable, Well-Defined Nickel(0) Catalysts for Catalytic C-C and C-N Bond Formation. *ACS Catal.* **2018,** *8*, 6606-6611.

8. Berini, C.; Winkelmann, O. H.; Otten, J.; Vicic, D. A.; Navarro, O., Rapid and Selective Catalytic Oxidation of Secondary Alcohols at Room Temperature by Using (N-Heterocyclic Carbene)-Ni-0 Systems. *Chem. Eur. J.* **2010,** *16*, 6857-6860.

9. (a) Nattmann, L.; Saeb, R.; Noethling, N.; Cornella, J., An Air-Stable Binary Ni(0)-Olefin Catalyst. *Nat. Catal.* **2020,** *3*, 6-13; (b) Tran, V. T.; Li, Z. Q.; Apolinar, O.; Derosa, J.; Joannou, M. V.; Wisniewski, S. R.; Eastgate, M. D.; Engle, K. M., Ni(Cod)(Dq): An Air-Stable 18-Electron Nickel(0)-Olefin Precatalyst. *Angew. Chem. Int. Ed.* **2020,** *59*, 7409-7413. (c) Tran, V.; Kim, N,; Rubel, C.; Wu, X.; Kang, T; Jankins, T.; Li, Z.-Q.; Joannou, M.; Ayers, S.; Gembicky, M. Bailey, J.; Sturgell, E.; Sanchez, B; Chen, J.; Lin, S.; Eastgate, M.; Wisniewski, S.; Engle, K. Structurally Diverse Bench-Stable Nickel(0) Pre-Catalysts: A Practical Toolkit for In Situ Ligation Protocols. *ChemRxiv*. **2022**, https://doi.org/10.26434/chemrxiv-2022-7zjvh.
10. (a) Iglesias, M. J.; Blandez, J. F.; Fructos, M. R.; Prieto, A.; Alvarez, E.; Belderrain, T. R.; Nicasio, M. C., Synthesis, Structural Characterization, and Catalytic Activity of IprNi(Styrene)(2) in the Amination of Aryl Tosylates. *Organometallics* **2012,** *31*, 6312-6316; (b) Wu, J. G.; Faller, J. W.; Hazari, N.; Schmeier, T. J., Stoichiometric and Catalytic Reactions of Thermally Stable Nickel(0) NHC Complexes. *Organometallics* **2012,** *31*, 806-809; (c) Elsby, M. R.; Johnson, S. A., Nickel-Catalyzed C-H Silylation of Arenes with Vinylsilanes: Rapid and Reversible Beta-Si Elimination. *J. Am. Chem. Soc.* **2017,** *139*, 9401-9407.
11. (a) Malik, H. A.; Sormunen, G. J.; Montgomery, J., A General Strategy for Regiocontrol in Nickel-Catalyzed Reductive Couplings of Aldehydes and Alkynes. *J. Am. Chem. Soc.* **2010,** *132*, 6304-6305; (b) Kuchenbeiser, G.; Donnadieu, B.; Bertrand, G., Stable Bis(Diisopropylamino)Cyclopropenylidene (Bac) as Ligand for Transition Metal Complexes. *J. Organomet. Chem.* **2008,** *693*, 899-904.
12. (a) Jenkins, A. D.; Robo, M. T.; Zimmerman, P. M.; Montgomery, J., Nickel-Catalyzed Three-Component Cycloadditions of Enoates, Alkynes, and Aldehydes. *J. Org. Chem.* **2020,** *85*, 2956-2965; (b) Jenkins, A. D.; Herath, A.; Song, M.; Montgomery, J., Synthesis of Cyclopentenols and Cyclopentenones Via Nickel-Catalyzed Reductive Cycloaddition. *J. Am. Chem. Soc.* **2011,** *133*, 14460-14466; (c) Ohashi, M.; Taniguchi, T.; Ogoshi, S., Nickel-Catalyzed Formation of Cyclopentenone Derivatives Via the Unique Cycloaddition of Alpha,Beta-Unsaturated Phenyl Esters with Alkynes. *J. Am. Chem. Soc.* **2011,** *133*, 14900-14903.
13. (a) Zimmerman, P. M., Single-Ended Transition State Finding with the Growing String Method. *J. Comp. Chem.* **2015,** *36*, 601-611; (b) Zimmerman, P. M., Growing String Method with Interpolation and Optimization in Internal Coordinates: Method and Examples. *J. Chem. Phys.* **2013,** *138*, 184102; (c) Zimmerman, P., Reliable Transition State Searches Integrated with the Growing String Method. *J. Chem. Theor. Comp.* **2013,** *9*, 3043-3050; (d) Dewyer, A. L.; Zimmerman, P. M., Finding Reaction Mechanisms, Intuitive or Otherwise. *Org. Biomol. Chem.* **2017,** *15*, 501-504; (e) Dewyer, A. L.; Arguelles, A. J.; Zimmerman, P. M., Methods for Exploring Reaction Space in Molecular Systems. *Wiley Interdisciplinary Reviews-Computational Molecular Science* **2018,** *8*.
14. Robo, M. T.; Frank, A. R.; Butler, E.; Nett, A. J.; Cañellas, S.; Zimmerman, P. M.; Montgomery, J., Activation Mechanism of Nickel(0) N-Heterocyclic Carbene Catalysts Stabilized by Fumarate Ligands. *ChemRxiv* **2021**, doi.org/10.26434/chemrxiv-22021-26433dgnf.

Synopsis TOC